ARCHIVE OF MECHANICAL ENGINEERING

DOI: 10.24425/ame.2023.144817 2023, Vol. 70, No. 2, pp. 199–218

Sylwester TUDRUJ [1], Krzysztof KUREC [2], Janusz PIECHNA [1], Konrad KAMIENIECKI [1]

Mass-Spring System (MSS) 3D simulation of a thin flexible membrane with a new model of the elasticity parameters

Received 15 July 2022, **Revised** 12 December 2022, **Accepted** 2 January 2023, **Published online** 30 March 2023

Keywords: Mass-Spring Systems (MSS), spring coefficient, physically based modeling, bubble inflation test

Mass Spring Systems (MSS) are often used to simulate the behavior of deformable objects, for example in computer graphics (modeling clothes for virtual characters) or in medicine (surgical simulators that facilitate the planning of surgical operations) due to their simplicity and speed of calculation. This paper presents a new, two-parameter method (TP MSS) of determining the values of spring coefficients for this model. This approach can be distinguished by a constant parameter which is calculated once at the beginning of the simulation, and a variable parameter that must be updated at each simulation step. The value of this variable parameter depends on the shape changes of the elements forming the mesh of the simulated object. The considered mesh is built of elements in the shape of acute-angled triangles. The results obtained using the new model were compared to FEM simulations and the Van Gelder model. The simulation results for the new model were also compared with the results of the bubble inflation test.

1. Introduction

Numerical simulations based on the MSS (Mass Spring System) method are successfully used in computer graphics. It owes its success to simplicity and ease of implementation and the calculation speed makes it suitable for real-time simulation.

✉ Sylwester TUDRUJ, e-mail: studruj@meil.pw.edu.pl

[1]Warsaw University of Technology, Institute of Aeronautics and Applied Mechanics, Warsaw, Poland. ORCIDs: S.T. 0000-0001-7487-9159; J.P. 0000-0003-4267-3994

[2]Warsaw University of Technology, Institute of Micromechanics and Photonics, Warsaw, Poland. ORCIDs: K.K. 0000-0002-5919-1206; K.K. 0000-0003-2481-4554

Two approaches to MSS type simulation are known. The first approach is referred to as position-based [1] and it focuses on the speed of calculations at the expense of lower accuracy. It is mainly used for simulations where visual effects are the most important, for example for modeling clothes [2–4]. The second approach is referred to as physically-based and it provides a greater accuracy.

The physically-based approaches to simulate deformable objects used continuum mechanical formulations where the governing equations were discretized and solved using numerical integration. An overview of physically-based (not just MSS) methods can be found in [5]. The MSS method has also found its applications in medicine. Based on this method, surgical simulators are created for planning and reviewing the effects of surgical operations, since simulation speed is highly desirable for this kind of simulations. A non-linear mass-spring model was also developed [6] in order to increase the accuracy of the simulation of soft tissue behavior and thus their realism.

In [7], an improved realistic mass-spring model is presented, which is mainly based on the three-dimensional theory of non-linear anisotropic elasticity of finite strains, used to simulate surgical operations based on virtual reality. In [8], a virtual pneumoperitoneum method was proposed that simulates the movement of the abdominal wall and viscera through a pneumoperitoneum based on mass-spring-damper (MSDM) models for planning laparoscopic surgeries. The paper [9] presents the development of a biomechanical model of large soft organs to simulate the interaction of the surgical gripper and the spleen in real time. In [10], a physical model with a new multi-component conical spring was proposed, which replaces the cylindrical spring of the traditional mass-spring model for simulating soft tissue virtual surgery. Paper [11] presents a virtual soft tissue cutting simulation system based on the mass-spring model for virtual surgery.

The scope of applicability of the MSS method is not limited to computer graphics and medical applications. In [12, 13] one can find examples of using this method to simulate the operation of airbags numerically.

The key issue in the simulation of real objects is the translation of their physical parameters, such as Young's modulus, into the parameters of the created MSS model (stiffness of the edges of the elements forming the mesh). One of the popular formulas used for this purpose is the formula proposed by Van Gelder [14], but the results obtained with it differ slightly from those obtained with the help of FEM. For example, in [15], aortic valve modeling was compared using MSS (thin flexible membrane based of Van Gelder formula) with FEM methods. Although the FEM method proved to be somewhat more accurate, the MSS calculations were significantly accelerated. In this work, the authors show that the newly proposed formula, at the expense of a certain complication of the model, gives results closer to those obtained with the help of both FEM and through the experiment.

2. Related work

In order to carry out a numerical simulation based on the MSS model, the physical parameters such as stiffness and a damping factor of the tested material must be replaced by the parameters appropriate for the model. There are two main methods for obtaining parameters of the MSS model (stiffness) from the physical properties of a material. The first one involves the use of experimental data, often in the form of video films showing the behavior of the test sample and such an adaptation of the spring coefficients as to obtain the most accurate representation of its actual behavior during the simulation. This adaptation is obtained by iterative route often using genetic algorithms [16]. The advantage of this method is therefore a faithful representation of the tested, real object. The disadvantage of this solution is due to the fact that it is closely matched to the specific material and the specific model being tested. Such an approach limits the possibility of using the method when one wants to introduce changes in the material or the experimental environment [17]. The experiment must then be run again to recalibrate the model.

The second approach is an analytical solution based on the physical properties of the material. A flat flexible membrane can be discretized in two ways. The first simple way is to use a triangular mesh which is made of one type of elastic elements (Fig. 1a).

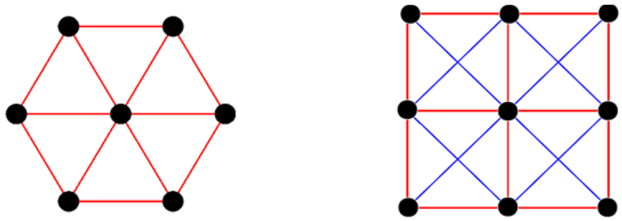

(a) (b)

Fig. 1. Types of meshes used in 2D cases: (a) triangular mesh with one type of elastic elements (springs); (b) quadrangular mesh with additional face diagonal elastic elements (blue) [17]

Quadrangular mesh with two types of springs such as edge springs and face diagonal springs (as shown in Fig. 1b) are rarely used. These two types of elastic elements may differ in their properties, i.e., the values of spring and damping coefficients. Different formulas for the values of spring coefficients for these two types of springs can be found in the following works: [18–20]. For triangular meshes, the spring coefficient can be calculated from the expression proposed by Van Gelder [14]:

$$k_c = \sum_{i=1}^{n} \frac{Et}{1+\nu} \frac{|T_i|}{c^2} + \frac{Et\nu}{1-\nu^2} \frac{a_i^2 + b_i^2 - c_i^2}{8\,|T_i|}, \tag{1}$$

with ν – the Poisson's ratio; E – Young's modulus of the simulated material; t – material thickness, a, b, c – respective sides lengths of a triangular element; T_i – i-th triangle; $|T_i|$ – surface area of the i-th triangle, $n = 2$ for 2D case (Fig. 2). In a simplified form, for $\nu = 0$, this formula takes the form [14]:

$$k_c = \sum_{i=1}^{n} Et \frac{|T_i|}{c^2} . \tag{2}$$

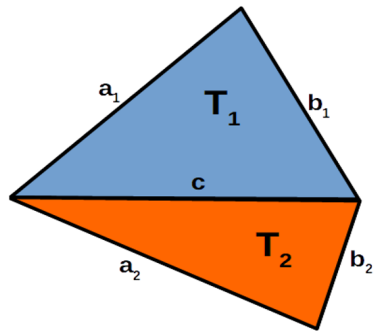

Fig. 2. Designations used in the Van Gelder model [14]

In the case of triangular meshes, a different, new approach was also proposed in the paper [19]. The spring coefficient can be calculated from the expression:

$$k_c = \sum_{i=1}^{n} Et \frac{\sqrt{3}}{4} . \tag{3}$$

The formula is correct provided that $\nu = \frac{1}{3}$ and the triangle is equilateral (Fig. 1a). For non-equilateral triangles, this formula can be modified to [19]:

$$k_c = \sum_{i=1}^{n} Et \frac{\sqrt{3}}{4} \frac{|T_i|}{|T_0|} , \tag{4}$$

where $|T_0|$ is the area of the equilateral triangle with side length c [19].

3. The proposed two-parameter model

A new model was proposed based on slightly different assumptions. The used geometrical parameters of the analyzed single triangle are shown in Fig. 3. In Fig. 3, the sides of a triangular element are marked as a, b, c, while angle measures are marked as α, β, γ and the heights of a triangle perpendicular to its sides are marked h_a, h_b, h_c, respectively.

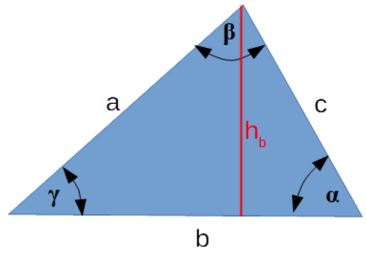

Fig. 3. A triangular element with marked angles, sides and one example height

Let the considered triangular element (element in the shape of acute-angled triangle) be a part of a rectangular piece of material, stretched in two perpendicular directions (see Fig. 4) (horizontal and vertical).

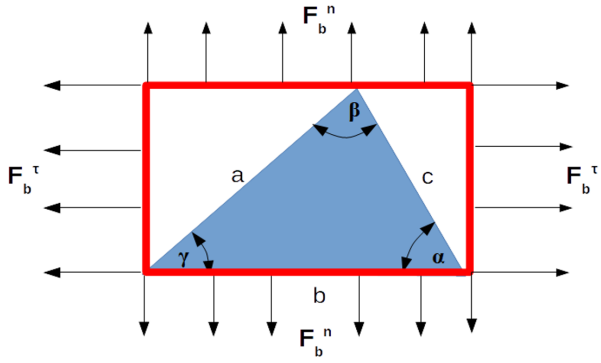

Fig. 4. A rectangular piece of material stretched in two perpendicular directions, by external forces, with a triangular element inside. F_b^n – normal force to edge b; F_b^τ – tangent force to the edge b

The value of the force resulting from the extension of the side b (in horizontal direction) of the triangular element can be represented by the formula:

$$F_b = k_b \Delta b = k_b \varepsilon_b^\tau b_0 \,, \tag{5}$$

where, k_b is the spring coefficient, Δb is the change in the length of the side b, b_0 is the initial length of side b, ε_b^τ is the tangent strain of the side b. The values of forces for sides a and c can be presented in a similar way. As a result of stretching a rectangular piece of material, a spring force perpendicular to the side b (F_b^n) will appear. Since the area of the triangular element under consideration is equal to half the surface area of the rectangular material fraction, therefore this area will be responsible for half the value of the F_b^n force. The part of this force resulting from the stretching of the triangular element can be represented as:

$$0.5F_b^n = (F_a \sin\gamma + F_c \sin\alpha) = \left(k_a \varepsilon_a^\tau a_0 \sin\gamma + k_c \varepsilon_c^\tau c_0 \sin\alpha\right). \tag{6}$$

The values of forces for sides a and c can be presented in a similar way. As a result of the action of the force F_b^n, the following stress will appear:

$$\sigma_b^n = \frac{F_b^n}{b_0 t} = \frac{E}{1-\nu^2}\left(\varepsilon_b^n + \nu\varepsilon_b^\tau\right), \tag{7}$$

where σ_b^n is normal stress to side b, t is material thickness, E is Young's modulus, ν is the Poisson's ratio, ε_b^n is normal strain to side b, ε_b^n can be represented as:

$$\varepsilon_b^n = \frac{\Delta h_b}{h_b}, \tag{8}$$

where Δh_b is a change in the height (h_b) of the triangular element. Similarly, stress values for sides a and c can be represented. In order to simplify the formula, the following designation was adopted:

$$q_b = \varepsilon_b^n + \nu\varepsilon_b^\tau, \tag{9}$$

where q_b will be called the variable factor of the spring coefficient of the side b. Using the equations (6), (7), (9) the values of the spring coefficients for individual sides of the triangular element can be represented as:

$$\begin{aligned}
k_a &= \frac{Et}{1-\nu^2}\,\frac{-a_0 q_a \sin\alpha + b_0 q_b \sin\beta + c_0 q_c \sin\gamma}{4a_0\varepsilon_a^\tau \sin\beta \sin\gamma},\\
k_b &= \frac{Et}{1-\nu^2}\,\frac{a_0 q_a \sin\alpha - b_0 q_b \sin\beta + c_0 q_c \sin\gamma}{4b_0\varepsilon_b^\tau \sin\alpha \sin\gamma},\\
k_c &= \frac{Et}{1-\nu^2}\,\frac{a_0 q_a \sin\alpha + b_0 q_b \sin\beta - c_0 q_c \sin\gamma}{4c_0\varepsilon_c^\tau \sin\alpha \sin\beta}.
\end{aligned} \tag{10}$$

The total value of given spring coefficients will be equal to the sum of the coefficients of neighboring triangular elements (similar to the Van Gelder Model, see Fig. 2 and Fig. 5).

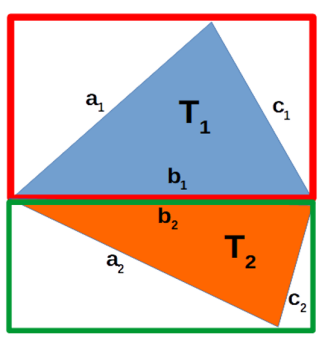

Fig. 5. Two adjacent triangular elements with their sides marked

After trigonometric transformations, the system of equations (10) can be written as:

$$
\begin{aligned}
k_a^t &= \sum_{i=1}^{n} \frac{Et}{8\left(1-\nu^2\right)|T_{0i}|} \frac{-a_{0i}^2 q_{ai} + b_{0i}^2 q_{bi} + c_{0i}^2 q_{ci}}{\varepsilon_{ai}^{\tau}}, \\
k_b^t &= \sum_{i=1}^{n} \frac{Et}{8\left(1-\nu^2\right)|T_{0i}|} \frac{a_{0i}^2 q_{ai} - b_{0i}^2 q_{bi} + c_{0i}^2 q_{ci}}{\varepsilon_{bi}^{\tau}}, \\
k_c^t &= \sum_{i=1}^{n} \frac{Et}{8\left(1-\nu^2\right)|T_{0i}|} \frac{a_{0i}^2 q_{ai} + b_{0i}^2 q_{bi} - c_{0i}^2 q_{ci}}{\varepsilon_{ci}^{\tau}},
\end{aligned}
\tag{11}
$$

where k_a^t, k_b^t, k_c^t correspond to total spring coefficients, $|T_{0i}|$ is the initial surface area of the i-th element and $i \in [1,\ 2]$. A fixed parameter was defined for the spring coefficient (12):

$$
Q_i = \frac{Et}{8\left(1-\nu^2\right)|T_{0i}|}, \tag{12}
$$

then the example equation from the equation system (11) can be written as:

$$
k_b^t = \sum_{i=1}^{n} Q_i q_i, \tag{13}
$$

where q_i is variable parameter for the spring coefficient (14):

$$
q_i = \frac{a_{0i}^2 q_{ai} - b_{0i}^2 q_{bi} + c_{0i}^2 q_{ci}}{\varepsilon_{bi}^{\tau}}. \tag{14}
$$

To sum up, the formula for the value of the spring coefficient consists of the product of two parts (13) (two-parameter model): a fixed part (12), which can be calculated once at the beginning of the simulation (Q_i), and a variable part (q_i), which must be updated at each time step (14). If the following condition is met:

$$
\varepsilon_a^{\tau} = \varepsilon_b^{\tau} = \varepsilon_c^{\tau} \tag{15}
$$

also if the strain values are equal to zero, the formula presented above (13) simplifies to the form:

$$
k_b^t = \sum_{i=1}^{n} Q_{0i}\left(a_{0i}^2 - b_{0i}^2 + c_{0i}^2\right), \tag{16}
$$

where:

$$
Q_{0i} = \frac{Et}{8(1-\nu)|T_{0i}|}. \tag{17}
$$

This additional formula (16) can be used to replace the basic equation (13) to avoid division by zero when there is no strain in the direction under consideration.

4. Numerical experiment

In order to verify the correctness of the developed model, a numerical experiment was carried out. In this experiment, the sphere subjected to internal pressure was examined. Due to the symmetry conditions of the examined object, it was decided to consider only a segment of the sphere (see Fig. 6).

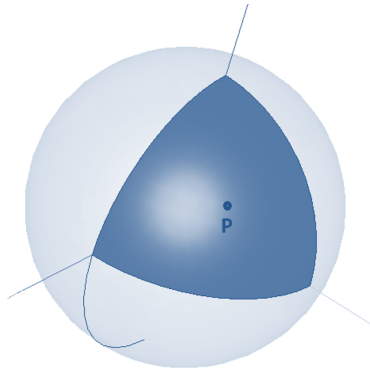

Fig. 6. A sphere made of flexible material
with a marked segment that has been tested.
P – point for measuring the sphere radius

FEM (Finite Element Method) calculations carried out in ANSYS were considered as a reference case. The results obtained with the use of the MSS (Mass Spring System) method were compared with the results from the reference case. Two cases were analyzed, in which the values of spring coefficients were obtained using both the Van Gelder method and a new method.

The simulations were carried out for a section of a sphere with a radius of one meter, loaded with $p = 10$ kPa pressure, for a material with a Poisson's ratio of $\nu = 0.3$. Several cases were tested for different values of Young's modulus and material thickness. The changes of the radius of the sphere segment were monitored.

Comparing the results of numerical simulations one can prove that the new, proposed by the authors model produces results closer to the FEM method than the Van Gelder model (Fig. 8). It has to be mentioned that the differences between the methods are small and both models produce results very similar to the FEM model (Table 1). In addition, it was noted that the new model compared with the classic approach is less sensitive to the mesh topology (Fig. 7).

Table 1. Comparison of MSS methods against the FEM method – relative error

	Van Gelder model (MSS) [%]	New model (MSS) [%]
$E = 50$ MPa, $d = 1$ mm	–0.65	–0.29
$E = 60$ MPa, $d = 1$ mm	–0.48	–0.19
$E = 60$ MPa, $d = 1.5$ mm	–0.27	–0.08

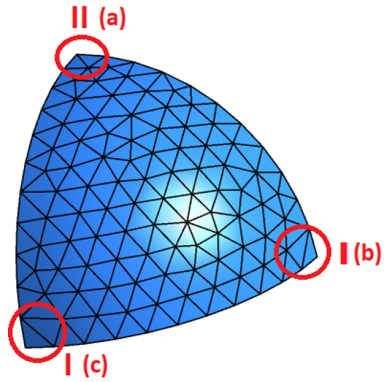

Fig. 7. Sphere segment with two types of mesh selected in its corners. Type II – corner a; type I – corners b and c

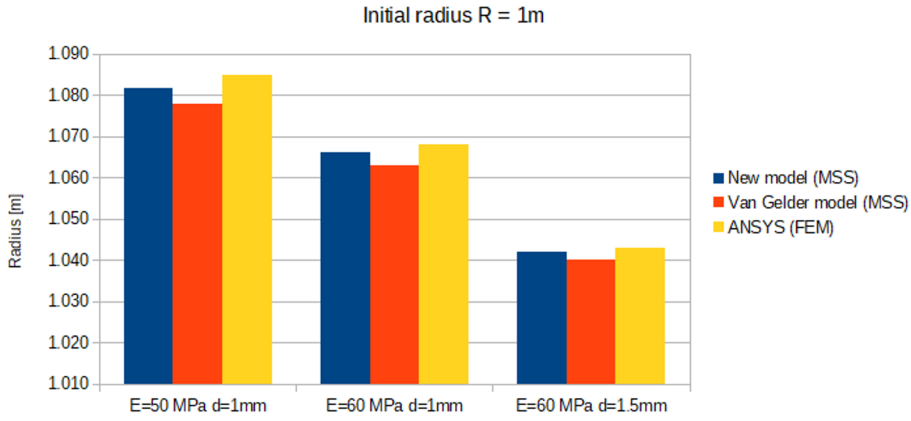

Fig. 8. Comparison of changes in radius values for different Young's moduli (E) and material thicknesses (d) for three calculation methods: FEM (ANSYS), MSS (Van Gelder model) and MSS (new model)

The differences in the values of the radius of the sphere segment obtained in its corners for different methods of meshing are smaller for the new model than for the Van Gelder model (Table 2).

Table 2. Differences in the values of the radius of the sphere section obtained in its corners for different methods of meshing. Comparison of the Van Gelder model with the new model. The simulation was carried out for Young's modulus equal to $E = 50$ MPa and material thickness $d = 1$ mm

	sphere radius [m]	sphere radius [m] at the corner a of type II	sphere radius [m] at the corner b of type I	sphere radius [m] at the corner c of type I
Van Gelder model	1.078	1.085	1.075	1.077
new model	1.082	1.083	1.079	1.079

5. Bubble inflation test

The next step in the verification of the newly developed model was to compare the behavior of the real object with its computer simulation. For this purpose, it was decided to carry out a bubble inflation test for a sample of the material made of rubber and reproduce its course using numerical simulation. Bubble inflation test is one of the methods used to test hyperelastic materials [21]. It involves subjecting thin material in the shape of a disk to high pressure (Fig. 9). This disc mounted on the edge bulges under pressure. By measuring the height of the resulting bubble, the strain-stress characteristics of the material under study can be obtained. Using the assumption that the resulting bubble is a thin-walled axial-symmetrical shell, the stress at its top can be expressed by the formula (18).

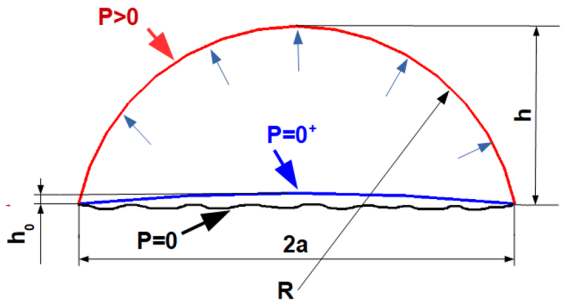

Fig. 9. Thin flexible membrane subjected to pressure: h – bubble height under high pressure ($P > 0$); h_0 – bubble height under pressure slightly higher than zero ($P = 0^+$); R – the radius of the bubble formed under the influence of high pressure ($P > 0$); a – radius of indistorted membrane; wrinkle condition for zero pressure ($P = 0$) [21]

$$\sigma_x = \sigma_y = \sigma = \frac{pR}{2t}, \tag{18}$$

where σ_x is the stress in the x direction, σ_y is the stress in the y direction, p is pressure, R – bubble radius, t – material disc thickness. In the case where the test sample at the beginning of the test is flat, the radius of curvature of the bubble is expressed by the formula (19) [22].

$$R = \frac{a^2 + h^2}{2h}, \tag{19}$$

where a is the radius of the disc, h – the height of the bubble formed under the influence of pressure. An important assumption is that the center-point displacement, h, must be lower than half the length of the membrane (i.e. $h < a$) [21]. In the case where the tested material is already pre-bulged (Fig. 9), the bubble

radius formula takes the form (20) [21]:

$$R = \frac{a^2 + (h + h_0)^2}{2\,(h + h_0)}\,, \tag{20}$$

where h_0 is the initial bubble height (Fig. 9). In this case, one can specify both the initial (21) and final (resulting from the action of pressure) (22) bubble arc length [21].

$$s_0 = \frac{a^2 + h_0^2}{h_0} \sin^{-1}\left(\frac{2ah_0}{a^2 + h_0^2}\right), \tag{21}$$

$$s_1 = \frac{a^2 + (h_0 + h)^2}{h_0 + h} \sin^{-1}\left(\frac{2a\,(h_0 + h)}{a^2 + (h_0 + h)^2}\right). \tag{22}$$

Using (21) and (22), the stretching ratio can be represented as (23):

$$\lambda = \frac{s_1}{s_0} \tag{23}$$

and strain (24).

$$\varepsilon = 1 - \lambda. \tag{24}$$

Using (18), (20) and (23) true stresses can be represented as [21]:

$$\Sigma = \lambda\sigma = \lambda\frac{pR}{2t} = \lambda\frac{p\left[a^2 + (h + h_0)^2\right]}{4\,(h + h_0)\,t}\,. \tag{25}$$

The data obtained from the bubble inflation test was used to define the properties of the material used in the numerical simulation.

6. Material properties

To create a spatial stress state model – as a material model for linearly elastic materials, it is enough to enter two quantities: Young's modulus E and Poisson's number ν [23]. In this case, strain in a given direction axis can be calculated from the relationship:

$$\begin{aligned}
\varepsilon_1 &= \frac{1}{E}\left[\sigma_1 - \nu\,(\sigma_2 + \sigma_3)\right], \\
\varepsilon_2 &= \frac{1}{E}\left[\sigma_2 - \nu\,(\sigma_1 + \sigma_3)\right], \\
\varepsilon_3 &= \frac{1}{E}\left[\sigma_3 - \nu\,(\sigma_1 + \sigma_2)\right].
\end{aligned} \tag{26}$$

For hyperelastic materials (for example rubber), the stress-strain relationship is non-linear (Fig. 10) [24]. In this case, to define such a material model, constitutive models are used. Such models are based on the so-called polynomials describing the density of strain energy W, accumulated in the volume of the material.

The amount of this energy describes the area under the curve graph (Fig. 10), and the stress-strain relationship is obtained from the dependence [25]:

$$W = f\left(I_1, I_2, I_3\right), \tag{27}$$

$$\sigma_{ij} = \frac{\partial W}{\partial \varepsilon_{ij}}, \tag{28}$$

where: I_1, I_2 and I_3 are the three invariants of the Green's deformation tensor, and:

$$\begin{aligned} I_1 &= \lambda_1^2 + \lambda_2^2 + \lambda_3^2, \\ I_2 &= \lambda_1^2\lambda_2^2 + \lambda_2^2\lambda_3^2, \\ I_3 &= \lambda_1^2\lambda_2^2\lambda_3^2, \end{aligned} \tag{29}$$

where: λ_1, λ_2, λ_3 – stretch ratios.

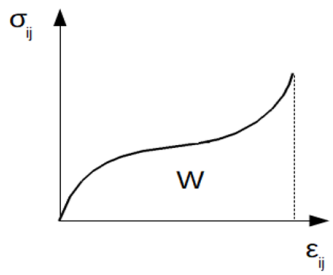

Fig. 10. Typical stress and strain characteristic of the hyperelastic material. The area under curve determines the amount of energy stored in hyperelastic material [23, 24]

Another approach is possible in the case of non-linear deformation characteristics. One can determine the Young's modulus in one of the following ways [26]:

- Tangent Young's modulus $E_{\tan}$ – at a fixed percentage of ultimate stress. It is defined as the slope of a line tangent to the stress-strain curve at a fixed percentage of the ultimate strength (Fig. 11a);
- Average Young's modulus E_{av} – of the straight-line part of a curve. The elastic modulus is defined as the slope of straight-line part of the stress-strain curve for the given test (Fig. 11b);
- Secant Young's modulus E_{sec} – at a fixed percentage of the final test. It is defined as the slope of the line from the origin (usually point (0, 0) to some fixed percentage ultimate strength, usually 50% (Fig. 11c).

For the purposes of this study, a model called the secant Young's modulus was chosen to describe the material properties of the tested material samples.

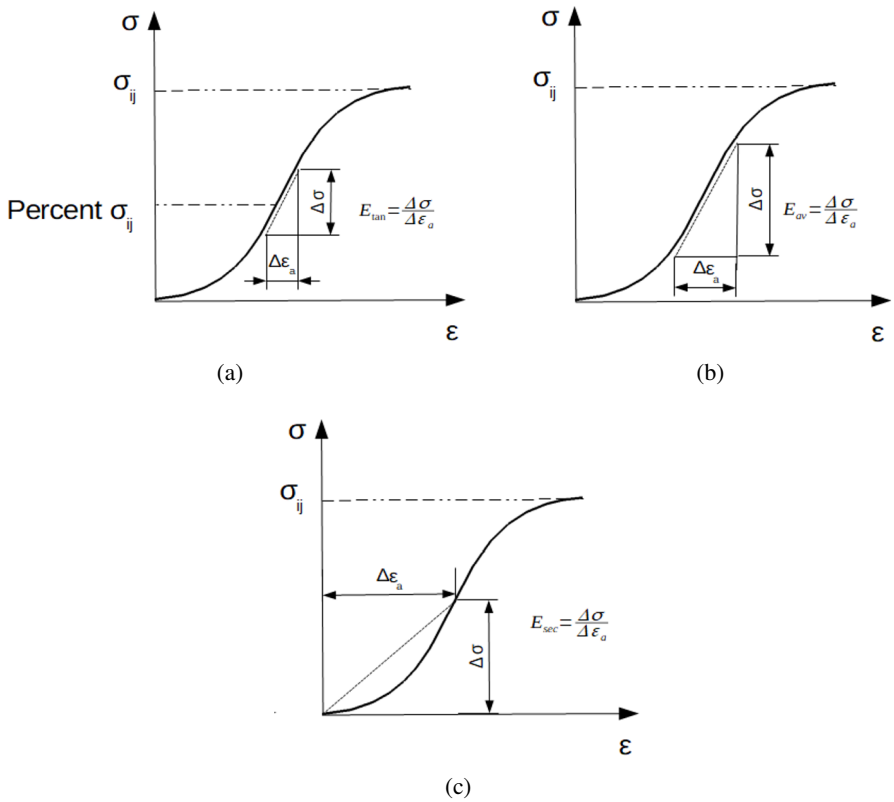

Fig. 11. (a) – Tangent Young's modulus ($E_{\tan}$); (b) – Average Young's modulus (E_{av}); (c) – Secant Young's modulus (E_{sec}) [26]

7. Experiment

As mentioned earlier, the bubble inflation test was also carried out to verify the newly developed model (Fig. 12). A $t = 0.35$ mm thick membrane made of latex rubber was tested. The diameter of the tested fragment of material was $D = 75$ mm. The tested membrane was attached to a two-inch pipe which was connected to a 150-liter air tank and a compressor. The tank was used to ensure that the membrane would only be subjected to semi-stationary pressure changes. There were no additional transient flow conditions such as pressure waves, because the large volume of the tank caused that the pressure increased slowly and evenly in it during the gas supply.

During the experiment, a series of photographs were taken showing the process of changing the shape of the flexible membrane. Computer image processing techniques were used to measure the bubble height. First, a special drawing was applied to previously taken pictures. This drawing was in the form of an elongated rectangle, inside which the top of the bubble could move. Then, a template was

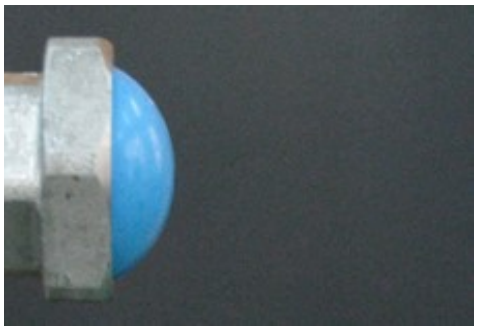

Fig. 12. View of the measuring station for the bubble inflation test, which consisted of a latex membrane attached to the compressed air supply pipe and a manometer

created, which was a small fragment of the photograph with a visible border between the bubble and the background inside the superimposed drawing. Using the CV2 numerical library and Python language, a script was written whose task was to find the template on each of the analyzed photographs (Fig. 13). This script gave the location of the template in the photograph in pixels. Knowing the real size of the characteristic elements of the photograph, the template position in pixels could be converted into meters.

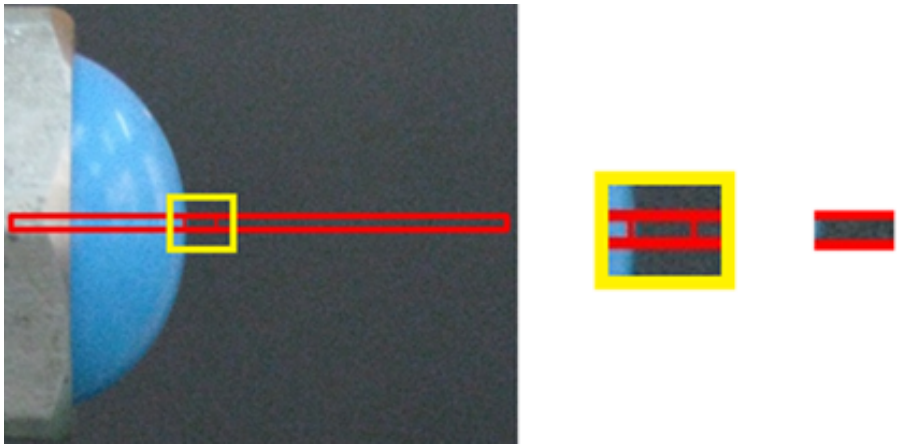

(a) (b) (c)

Fig. 13. Finding the location of the template in the photograph. (a) a template tailored to the photograph using a script written in Python; (b) enlarged area representing the template tailored to the photo; (c) template

Based on the experiment, a stress-strain relationship diagram was created for the tested material (Fig. 14). It can be seen that this relationship is non-linear.

For the purposes of this study, the dependence of Young's modulus value on strain ($E_{\text{sec}}^{\varepsilon}$) was defined (for the 2D case). This relationship was modeled using the secant Young's modulus. The difference is that this relationship was not limited to

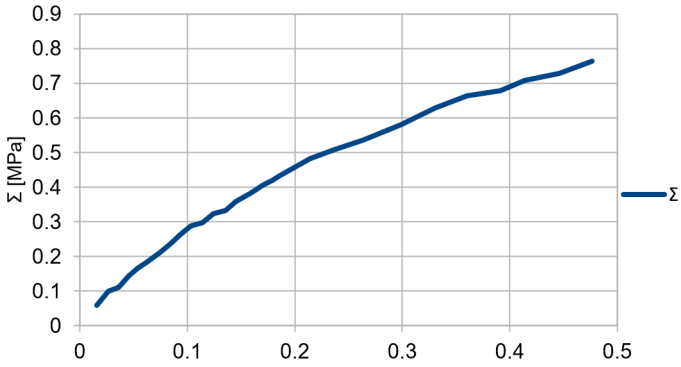

Fig. 14. Stress-strain curve for the tested material from which the flexible membrane was made

calculating the value of this module for one deformation value, but it was calculated for individual deformation values from their entire range. This relationship (Fig. 15) was then approximated using a quartic polynomial curve.

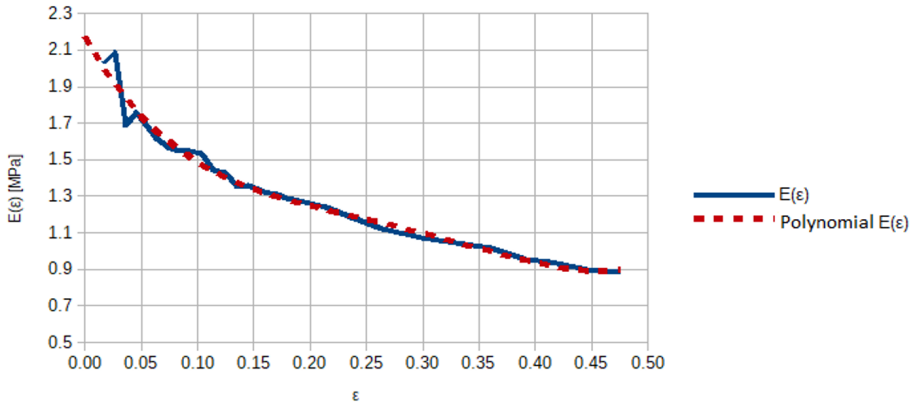

Fig. 15. Dependency: strain – Young's modulus. $E(\varepsilon)$ – experiment; polynomial $E(\varepsilon)$ – an approximation curve of the experiment results

The equation of polynomial curve was then used during numerical simulation to determine the Young's modulus value for the appropriate deformations of the tested material. Based on the work [22], the value of the Poisson's ratio for the tested material was set at $\nu = 0.45$. Two types of simulations were carried out, one based on the Van Gelder model and the other based on the new model (TP MSS).

The results of numerical simulations were compared with the results of the experiment (Fig. 16 and Fig. 17).

The parameter that was analyzed was the height h of the bubble formed from the membrane under the influence of pressure The results obtained using the new model are closer to the reference results than those when using the Van Gelder model (Fig. 17 and Table 3).

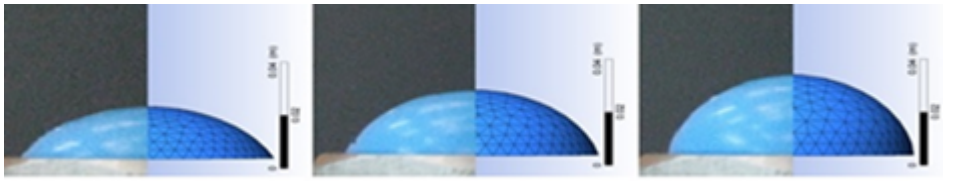

(a) (b) (c)

Fig. 16. Comparison of the results of the numerical simulation (new MSS model) with the experiment for different pressure values. (a) 5000 Pa; (b) 7300 Pa; (c) 8940 Pa

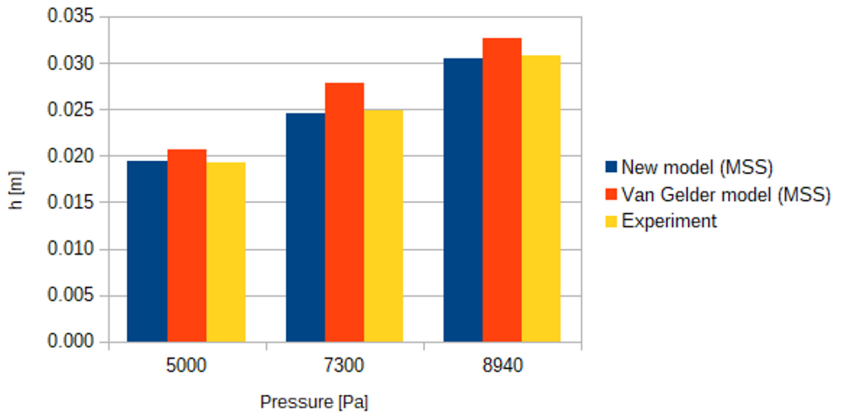

Fig. 17. Comparison of the results of the experiment with numerical simulations for different pressure values; h – bubble height

Table 3. Comparison of MSS methods with experiment – relative error

Pressure [Pa]	Van Gelder model (MSS) [%]	New model (MSS) [%]
5000	8.07	1.50
7300	11.69	–1.20
8940	6.39	–0.87

The authors are convinced that the bubble inflation test is a good test to verify the correctness of the method. As mentioned earlier, the test sample subjected to stretching is fixed on its edge. Of course, in the MSS simulation while reproducing the course of this test, the edge of the material must also be fixed. It means that the triangular elements adjacent to this edge must have one locked edge (its length does not change) and the other two edges can be freely stretched. So, we have to do stretching in one direction to the center of the sample. As one moves away from the edge of the specimen, stretching initially occurs in a direction transverse to specimen's radius (and gradually increases) until the specimen is stretched uniformly in all directions in the center (Fig. 18). Thanks to this, the

final simulation result (the shape of the sample under pressure and the height of the resulting bubble) depends on the correct mapping of the shape changes of triangular elements stretched in a different range and in different directions.

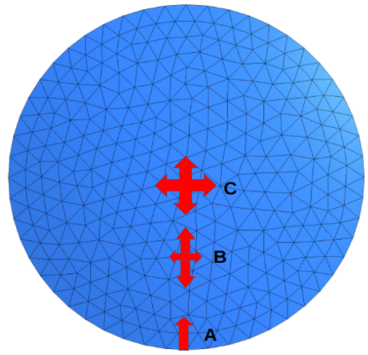

Fig. 18. Sample stretching areas during bubble inflation test: A – fixed edge, sample only stretched centripetally; B – the advantage of centripetal stretching over the transverse; C – uniform stretching in all directions

8. Parachute – sample result of a simulation using the Two-Parameter Mass-Spring System

The authors use the newly developed formula to conduct numerical simulations of the FSI type (Fluid Structure Interaction). The CFD Ansys-Fluent [27] program is the basis for these simulations. This program provides a tool called UDF (User Defined Function). This tool allows one to implement useful, not intended by its authors functionality into the program. By using this tool, the possibility of performing FSI simulations of thin deformable membranes based on the newly developed Two-Parameter Mass-Spring System (TP MSS) was added to the Ansys-Fluent program.

The examples presented so far have focused on the fixed shape of the membrane under the influence of pressure on it. The modified program can also be used to study dynamic phenomena, such as filling the parachute canopy (Fig. 19).

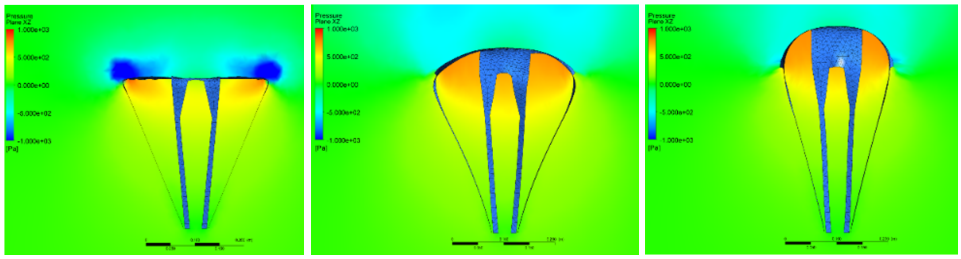

Fig. 19. Stages of filling a cross-type parachute canopy. FSI simulation using TP MSS

9. Conclusion

The conducted research confirms that the newly proposed MSS model may be a valuable replacement for the previously used models, especially in the case when the accuracy of calculations and compliance with reality are particularly desirable. Although in the presented examples the model proposed by the authors turned out to be better than the Van Gelder model, it requires further research and testing on a larger number of cases. In the case of a numerical experiment in which the sphere evenly stretched in all directions was studied, the new model was only slightly better (smaller relative error) than the previous one (Van Gelder). However, it is worth emphasizing that in this case the advantage of the new model was the lower sensitivity to the changes in the topography of the mesh. Larger differences between the models were revealed when comparing the simulation results with the bubble inflation test. This larger difference in the results between the models, in the case of the experiment, is due to the fact that the van Gelder model is valid for Poisson's ratio equal to 0.3 [28], and the value of 0.45 was used in the experiment.

The new model is better (much smaller relative error) than the Van Gelder model in mapping the behavior of real, unevenly stretched material in the form of a thin rubber disk. The indicated increase in solution accuracy obtained with the new method will be particularly appreciated in medical applications using the MSS method.

Acknowledgements

This project was funded by the National Centre for Research and Development, grant number PBS3/B6/34/2015, "Aktywny system tłumienia drgań pojazdu" ("The active system of car body oscillation damping").

References

[1] J. Bender, M. Muller, M.A. Otaduy, M. Teschner, and M. Macklin. A survey on position-based simulation methods in computer graphics. *Computer Graphics Forum*, 33(6):228–251, 2014. doi: 10.1111/cgf.12346.

[2] X. Provot. Deformation constraints in a mass-spring model to describe rigid cloth behaviour. In: *Proceedings of Graphics Interface '95*, pages 147–154, Quebec, Canada, 1995. doi: 10.20380/GI1995.17.

[3] T.I. Vassilev, B. Spanlang, and Y. Chrysanthou. Efficient cloth model and collisions detection for dressing virtual people. In: *Proceeding of ACM/EG Games Technology*, Hong Kong, 2001.

[4] Z. Cao and B. He. Research of fast cloth simulation based on mass- spring model. In: *Proceedings of the 2012 National Conference on Information Technology and Computer Science*, pages 467–471, 2012. doi: 10.2991/citcs.2012.121.

[5] A. Nealen, M. Müller, R. Keiser, E. Boxerman, and M. Carlson. Physically based deformable models in computer graphics. *Computer Graphics Forum*, 25(4):809–836, 2006. doi: 10.1111/j.1467-8659.2006.01000.x.

[6] E. Basafa, F. Farahmand, and G. Vossoughi. A non-linear mass-spring model for more realistic and efficient simulation of soft tissues surgery. *Studies in Health Technology and Informatics*, 132:23–25, 2008.

[7] S. Xu, X. P. Liu, H. Zhang, and L. Hu. An improved realistic mass-spring model for surgery simulation. In: *2010 IEEE International Symposium on Haptic Audio Visual Environments and Games*, Phoenix, USA, 2010. doi: 10.1109/HAVE.2010.5623989.

[8] Y. Nimura, J. D. Qu, Y. Hayashi, M. Oda, T. Kitasaka, M. Hashizume, K. Misawa, and K. Mori. Pneumoperitoneum simulation based on mass-spring-damper models for laparoscopic surgical planning. *Journal of Medical Imaging*, 2(4):044004, 2015. doi: 10.1117/1.JMI.2.4.044004.

[9] H. Dehghani Ashkezari, A. Mirbagheri, S. Behzadipour, and F. Farahmand. A mass-spring-damper model for real time simulation of the frictional grasping interactions between surgical tools and large organs. *Scientia Iranica*, 22(5):1833–1841, 2015.

[10] B. Dong, J. Li, G. Yang, X. Cheng, and Q. Gang. A multi-component conical spring model of soft tissue in virtual surgery. *IEEE Access*, 8:146093–146104, 2020. doi: 10.1109/ACCESS.2020.3014730.

[11] X. Zhang, J. Duan, W. Sun, T. Xu, and S.K. Jha. A three-stage cutting simulation system based on mass-spring model. *Computer Modeling in Engineering & Sciences*, 127(1):117–133, 2021. doi: 10.32604/cmes.2021.012034.

[12] S. Tudruj and J. Piechna. Numerical analysis of the possibility of using an external air bag to protect a small urban vehicle during a collision. *Archive of Mechanical Engineering*, 59(3): 257–281, 2012. doi: 10.2478/v10180-012-0013-2.

[13] J. Piechna, T. Janson, P. Sadowski, S. Tudruj, A. Piechna, and L. Rudniak. Numerical study of aerodynamic characteristics of sports car with movable flaps and deformable airbags. In: *Proceedings of Automotive Simulation World Congress*, Frankfurt, Germany, 2013.

[14] A. Van Gelder. Approximate simulation of elastic membranes by triangulated spring meshes. *Journal of Graphics Tools*, 3(2):21–41, 1998. doi: 10.1080/10867651.1998.10487490.

[15] P. E. Hammer, M.S. Sacks, P.J. del Nido, and R.D. Howe. Mass-spring model for simulation of heart valve tissue mechanical behavior. *Annals of Biomedical Engineering*, 39(6):1668–679, 2011. doi: 10.1007/s10439-011-0278-5.

[16] J. Louchet, X. Provo, and D. Crochemore. Evolutionary identification of cloth animation models. In: D. Terzopoulos, D. Thalmann, (eds.) *Computer Animation and Simulation'95*, pages 44–54, Springer, 1995. doi: 10.1007/978-3-7091-9435-5_4.

[17] K. Golec. *Hybrid 3D Mass Spring System for Soft Tissue. Modeling and Simulation*. Ph.D. Thesis, Université de Lyon, France, 2018.

[18] V. Baudet, M. Beuve, F. Jaillet, B. Shariat, and F. Zara. Integrating tensile parameters. In *WSCG'2009*, 2009, hal-00994456.

[19] B.A. Lloyd, G. Székely, and M. Harders. Identification of spring parameters for deformable object simulation. *IEEE Transactions on Visualization and Computer*, 13(5):1081–1094, 2007. doi: 10.1109/TVCG.2007.1055.

[20] S. Natsupakpong and M.C. Çavusoglu. Determination of elasticity parameters in lumped element (mass-spring) models of deformable objects. *Graphical Models*, 72(6): 61–73, 2010. doi: 10.1016/j.gmod.2010.10.001.

[21] W.P. Jackson. *Characterization of Soft Polymers and Gels using the Pressure-Bulge Technique*. Ph.D. Thesis, California Institute of Technology, Pasadena, USA, 2008.

[22] L. Wanigasooriya. *Mechanical Characterisation and Ram Extrusion of Wheat Flour Dough*. Ph.D. Thesis, Imperial College London, UK, 2006.

[23] P. Jaszak. Modelling of the rubber in Finite Element Method. *Elastomery*, 20(3):31–39, 2016. (in Polish).

[24] R. Jakel. Analysis of hyperelastic materials with MECHANICA. Presentation for 2nd SAXSIM Technische Universität Chemnitz, Germany, 2010.

[25] A. Ali, M. Hosseini, and B.B. Sahari. A review of constitutive models for rubber-like materials. *American Journal of Engineering and Applied Sciences*, 3(1):232–39, 2010. doi: 10.3844/ajeassp.2010.232.239.

[26] P. Małkowski and Ł. Ostrowski. The methodology for the young modulus derivation for rocks and its value. *Procedia Engineering*, 191:134–141, 2017. doi: 10.1016/j.proeng.2017.05.164.

[27] Ansys [Online]. Available: www.ansys.com.

[28] M. Kot, H. Nagahashi, and P. Szymczak. Elastic moduli of simple mass spring models. *The Visual Computer*, 31:1339–1350, 2015. doi: 10.1007/s00371-014-1015-5.